Evidence of thermal transport anisotropy in stable glasses of vapor deposited organic molecules

Joan Ràfols-Ribé,[1] Riccardo Dettori,[2] Pablo Ferrando-Villalba,[1] Marta Gonzalez-Silveira,[1] Llibertat Abad,[3] Aitor F. Lopeandía,[1] Luciano Colombo,[2] and Javier Rodríguez-Viejo[1,*]

[1]*Nanomaterials and Microsystems Group, Physics Department, Universitat Autònoma de Barcelona, 08193 Bellaterra, Spain*

[2]*Department of Physics, University of Cagliari, Cittadella Universitaria, 09042 Monserrato (Ca), Italy*

[3]*IMB-CNM-CSIC, Campus Bellaterra, 08193 Bellaterra, Spain*

(Received 27 October 2017; published 29 March 2018)

Vapor deposited organic glasses are currently in use in many optoelectronic devices. Their operation temperature is limited by the glass transition temperature of the organic layers and thermal management strategies become increasingly important to improve the lifetime of the device. Here we report the unusual finding that molecular orientation heavily influences heat flow propagation in glassy films of small molecule organic semiconductors. The thermal conductivity of vapor deposited thin-film semiconductor glasses is anisotropic and controlled by the deposition temperature. We compare our data with extensive molecular dynamics simulations to disentangle the role of density and molecular orientation on heat propagation. Simulations do support the view that thermal transport along the backbone of the organic molecule is strongly preferred with respect to the perpendicular direction. This is due to the anisotropy of the molecular interaction strength that limits the transport of atomic vibrations. This approach could be used in future developments to implement small molecule glassy films in thermoelectric or other organic electronic devices.

DOI: 10.1103/PhysRevMaterials.2.035603

I. INTRODUCTION

Organic glasses are important for a wide range of scientific and technological processes [1]. Their utilization in organic electronics applications such as organic light-emitting devices [2] (OLEDs) is no longer a lab curiosity but rather a mature technology for high-performance displays [2,3]. However, solid-state lightning applications that require high brightness are still to be realized due to the insufficient thermal stability of the organic materials. Thermal stress and degradation [4], together with the fact that the luminance and lifetime of OLED devices decrease when operated at high temperatures [5], are widely reported facts. In this respect, an appropriate understanding of thermal transport may help designing materials with tailored heat dissipation characteristics to minimize heat accumulation in OLEDs [6,7] or to reduce heat flow while increasing charge transport in search for potential thermoelectric applications [8–11]. Their semiconductor nature and the low thermal conductivities make them suitable candidates to improve the thermoelectric figure-of-merit ZT. We note most of the previous studies in this direction have been reported for polymer-based devices and fewer on small molecule organic semiconductors [12].

Physical vapor deposition has been shown to be a suitable tool to tailor the properties of the deposited layers, not only for organic semiconductors [13,14], but also for many other small organic molecules [15–20]. When the deposition conditions, basically substrate temperature and growth rate, are properly set, glasses with exceptional thermodynamic and kinetic stability [13,15,21,22], high densities [14,23–25], low heat capacities [17,26], low water uptake [27], or high moduli [28] can be obtained. These glasses, dubbed ultrastable, are currently gaining widespread attention within the glass community, and a recent report demonstrates the improved packing of these glasses can yield to outstanding improvements in OLED efficiency [29]. An interesting feature of some vapor deposited organic glasses is that molecules can have average spatial orientations that differ from the random distribution of an isotropic glass. Recent studies have started to focus on the molecular orientation in those materials and its influence on the efficiency of OLEDs [30]. The existence of molecular packing anisotropy in vapor deposited organic semiconductor thin film glasses was first identified by Lin *et al.* [31]. Yokoyama and coworkers [32,33] studied the degree of orientation depending on the molecular aspect ratio of the molecule and the deposition conditions. Dalal *et al.* [13] performed dichroism and birefringence measurements on several organic semiconductors, and proposed the ratio between the deposition temperature and the glass transition temperature, T_{dep}/T_g, to be the primary parameter affecting the molecular orientation. It is now well established that most of the studied vapor deposited organic glasses show anisotropic packing and, in particular, that the lower the substrate temperature during growth, the higher is the tendency towards horizontal orientation [34]. This tunable molecular orientation provides new opportunities to tailor the electrical, thermal, and optical properties of the glassy materials.

Many previous studies have focused on the electronic transport properties of organic glasses and crystals, since this is a key parameter for the use of these materials in optoelectronic devices [35]. On the contrary, thermal conductivity measurements in small molecule organic glasses remains largely unexplored and only few studies are reported [36,37].

*Corresponding author: javier.rodriguez@uab.es

In general, it is well known that increasing disorder has a remarkable effect on the thermal conductivity. For an inorganic material, such as silicon, the thermal conductivity varies from 150 $W\,m^{-1}\,K^{-1}$ in bulk Si to around 1.4 $W\,m^{-1}\,K^{-1}$ for the disordered material [38,39]. This low value is frequently understood through the theory of the minimum thermal conductivity where atomic vibrations with mean free paths of the order of the interatomic distance contribute to heat transport [40]. In organic materials the van der Waals interactions between molecules have a remarkable effect on heat propagation and disorder plays a comparatively less dramatic effect on the thermal conductivity compared to their crystalline counterparts. However, the current understanding of heat conduction in organic glasses is limited by the largely incomplete knowledge about the actual mechanisms ruling over thermal energy exchange in these systems and how the glass atomic-scale morphology affects transport. Measurements on thin-film organic crystals although more abundant also lack a proper understanding of how crystal anisotropy may affect thermal transport along and perpendicular to the molecular chain. The growth of large crystals to minimize the strong influence of grain size on phonon transport is a requirement to unveil the role of crystal anisotropies in heat flow propagation. Ac-calorimetry was previously used to extract the thermal diffusivity of rubrene layers [41]. In this material, the in-plane thermal diffusivity is higher than the through-plane, indicating poor thermal transport across the phenyl groups of the rubrene molecules. On the contrary, measurements on 6,13-Bis(triisopropylsilylethynyl)pentacene, TIPS-pn, show the through-plane thermal diffusivity is larger than the in-plane one due to an excellent π-orbital overlap [42]. The role of thermal anisotropy has been already addressed in polymeric samples [43] where rubbing or stretching has been used to produce the alignment of the backbone of the polymer along the fiber direction. In this case, the conductivity along the axis of the polymeric chain can be up to 20 times higher than in the perpendicular direction [44].

One difficulty towards a comprehensive analysis of thermal conductivity anisotropies arises from the lack of appropriate experimental techniques to measure the in-plane thermal transport in thin films. Previous in-plane measurements on polymers or polymer nanofibers were conducted on suspended structures [44,45] that directly provide the in-plane thermal conductance. This methodology, frequently used for inorganic nanowires of low thermal conductance, requires lengthy or sophisticated approaches to precisely place the sample bridging the heater/sensor platforms. We have recently shown that a modification of the 3ω-Völklein technique [46–49] can be used to monitor in real time the growth of organic layers and to measure their in-plane thermal conductance [48]. The high sensitivity of the technique and its versatility makes it an ideal tool to explore the in-plane thermal transport characteristics of organic thin films.

Here we show that by changing the deposition temperature of vapor-deposited glassy films of an organic semiconductor, the thermal anisotropy ratio, defined as the relative difference between in-plane $k_\parallel$ and through-plane $k_\perp$ conductivity, $(k_\parallel - k_\perp)/k_\perp$, can be modified to nearly 40%. The achievement of substantial thermal anisotropy in small molecule thin-film glasses is counter-intuitive since structural disorder should lower the anisotropy ratio. By comparing our experimental data with molecular dynamics simulations mimicking the orientation of the vapor deposited organic layers, we disentangle the role of density and molecular orientation on heat propagation. We provide evidence that the change of thermal conductivity is mainly driven by the molecular packing anisotropy in the glass and that thermal transport along the N-N backbone of the N,N′-Bis(3-methylphenyl)-N,N′-bis(phenyl)-benzidine, TPD, molecule is strongly preferred with respect to the perpendicular direction due to a stronger molecular interaction in the former.

II. METHODS

A. Experimental

1. Sample preparation

A hole transport molecule, N,N′-Bis(3-methylphenyl)-N,N′-bis(phenyl)-benzidine (TPD) was purchased from Cymit Quimica S.L. (>99%, purified by sublimation) and used without further purifications. The glass transition T_g of the TPD was found to be 333 K, measured by differential scanning calorimetry (DSC) for a sample cooled and heated at 10 K/min (see Fig. S3 in Ref. [50]). Thin layers of this material, with thicknesses ranging from 150 to 340 nm, were grown by thermal evaporation in a UHV chamber at a base pressure of 5×10^{-8} mbar using an effusion cell (CREATEC). The deposition rate was monitored using a quartz crystal microbalance (QCM) located close to the substrate and kept constant at 0.21 ± 0.02 nm/s by controlling the effusion cell temperature. The QCM true rate was previously calibrated by measuring a reference sample at the profilometer. The samples were deposited directly onto the silicon nitride membrane-based sensor and subsequently measured in differential mode using the 3ω-Völklein [46–49] method. The sensors, a sample, and a reference were placed on a substrate with a heating element and a Pt100 and the temperature was controlled during the deposition and the measurement of the films. The deposition temperatures ranged from 220 to 330 K that is 0.6 to 0.99 times their glass transition temperature. After each deposition, the substrate temperature was always set back to 296 K for the thermal conductivity measurements.

2. Thermal conductivity measurements

Out-of-plane: 3ω. The through-plane thermal conductivity was measured with the differential *3ω* method. We used 100-nm-thick Al wires with a 5-nm Cr adhesion layer for the *3ω heater/*sensor. The thin film heater of width 5 μm and length 2 mm was defined through the use of a shadow mask during deposition. All measurements were carried out at 290 K in a vacuum of 2.5×10^{-7} mbar. Joule heating was produced by applying an ac current to the Al strip using a Keithley 6221 source on the current pads of the sensor. The *3ω* voltage was measured using instrumentation amplifiers in a differential measurement with a National Instruments DAQ. The one-dimensional steady-state heat conduction model was used to extract the cross-plane thermal conductivity values from the temperature rise of the films (see Ref. [50]). Measurements were conducted on samples grown at 220 and 304 K.

In-plane measurements: 3ω-Völklein. We use a modification of the 3ω-Völklein method [48] previously developed

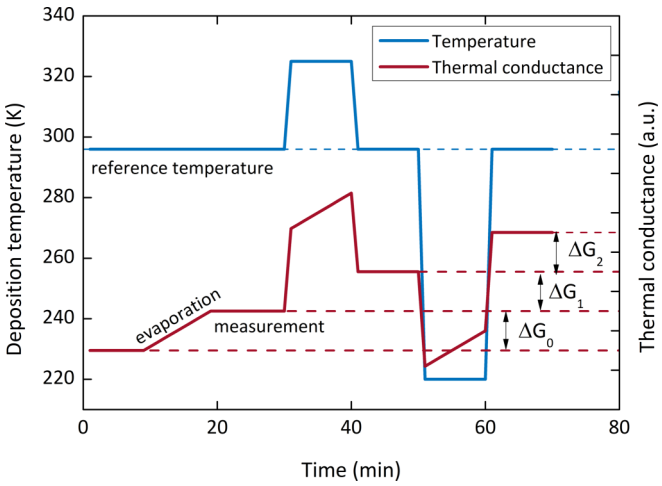

FIG. 1. Measurement procedure of the in-plane thermal conductance. Scheme of the procedure followed to evaluate the thermal conductance of a multilayer stack. The substrate was set to the deposition temperature (in blue) and subsequently cooled or heated at the reference temperature of 295 K. The conductance value is obtained from the differential value before and after the measurement (in red).

by Völklein *et al.* [49]. In Ref. [50], we provide details of the technique. Briefly, in this setup, we use a silicon nitride membrane with the same symmetry as a metal wire that is used for heating/sensing (Fig. S4 in Ref. [50]). The sensor is operated in differential mode, which allows to measure *in situ* the conductance with a very high sensitivity $\Delta k/k \simeq 10^{-3}$. We have measured the in-plane thermal conductance of thin films of TPD and α-NPD (shown in Ref. [50]) deposited over a wide temperature range, from 220 to 333 K. To obtain the conductance at each T_{dep}, we use two different approaches. The first one consists of a single measurement in which 340 nm of TPD are evaporated onto the sensor and subsequently measured. After depositing each film at a given temperature, the sensor is removed from the chamber, cleaned and prepared for the following evaporation. Figure 2 shows (in blue) the thermal conductance G as a function of the deposition temperature obtained using this approach. In the second approach, G was measured at a reference temperature in between depositions at different temperatures of 150-nm-thick layers. The layer conductance was, therefore, obtained as the differential measurement before and after each deposition, as sketched in Fig. 1.

B. Computational

Force field. The TPD molecule is modeled according to the CVFF [51] force field, where cross-coupling terms between the various bonded terms provide an accurate description of intramolecular interactions. The nonbonded interactions are in turn described by a superposition of a Lennard-Jones potential (addressed to describing the van der Waals contribution) and of a Coulomb term as follows:

$$\sum\left(\frac{A}{r^{12}}-\frac{B}{r^{6}}\right)+\sum\frac{q_i q_j}{r},$$

where the sum is performed over all the pairs of nonbonded atoms. The Lennard-Jones term is truncated by a cutoff set at 10.0 Å, while a particle-particle particle-mesh solver approach is adopted to solve the electrostatic problem in the reciprocal space. Coulomb interactions are calculated by assuming fixed charges, as previously obtained by fitting the electrostatic potential of an all-electron Hartree−Fock calculation performed with a medium-sized basis set 6–31G*. The fitting was performed using the RESP method [52,53]. Finally, the Tersoff [54] force field is adopted to describe the silicon substrate, giving such bond-order potential also the role of describing the interactions among molecular carbon atoms and silicon atoms in the substrate.

Molecular dynamics simulations. Molecular dynamics simulations are executed by LAMMPS [55] package. Equations of motion are integrated according to the velocity-Verlet integration scheme with a time step of 0.5 fs. Time integration is performed on Nosé-Hoover non-Hamiltonian equations for both constant-pressure (NPT) and constant-temperature (NVT) runs, respectively, used to reach equilibrium density at a given temperature and to further equilibrate the sample at a given temperature. Thermostatting and barostatting are achieved by a coupling parameter of 50.0 fs and a relaxation time of 500.0 fs, respectively.

Sample preparation. For the anisotropic samples, in order to enforce a preferential molecular orientation parallel to the Si substrate, a layer-by-layer deposition was performed: a first layer of 47 molecules was placed on top of a $20a_0 \times 20a_0$ substrate (where $a_0 = 5.4305$ Å is the equilibrium silicon lattice constant for Tersoff potential), followed by a geometry optimization and a low temperature ($T = 1$ K) annealing for 100 ps. As for *xy-ISO* samples there was no in-plane order, while in the *ANIS* samples, molecular axes were mainly oriented along an in-plane direction. This procedure was then repeated piling up to 16 layers: at each step, the whole structure was very carefully relaxed. This effectively generated a 6.9-nm-thick film of 752 TPD molecules, which resulted in being aligned parallel to the substrate. Eventually, the final sample was gently heated up (at 10^{-4} K/fs rate) and then equilibrated (400 ps + 100 ps) at the measurement temperature, obtaining a density in the range 1.080–1.085 g/cm^3, for the *ANIS* samples, and 1.069–1.079 g/cm^3 for the *xy-ISO*. Representative views of the structures are shown in Fig. S5. Further details are provided in Ref. [50].

As for the isotropic case, the *xy-ISO* sample was used as a starting configuration: the deposited film was heated up to 900 K during a 300-ps-long NVT run, and then annealed at that temperature for further 500 ps. This allowed the TPD film to completely lose its previous anisotropic structure. We have carefully monitored the molecular orientation on-the-fly to control that a fully isotropic sample was indeed forming. The TPD film was then cooled (at 10^{-4} K/fs rate) and then equilibrated at the measurement temperature, resulting into a density in the range 1.059–1.065 g/cm^3.

Calculating thermal conductivity. The thermal conductivity tensor $\overleftrightarrow{k}$ of a system of volume V is calculated according to the Green-Kubo formalism:

$$k_{\alpha\alpha}=\frac{1}{k_B T^2 V}\int_0^{\infty}\langle J_\alpha(0)J_\alpha(t)\rangle dt,$$

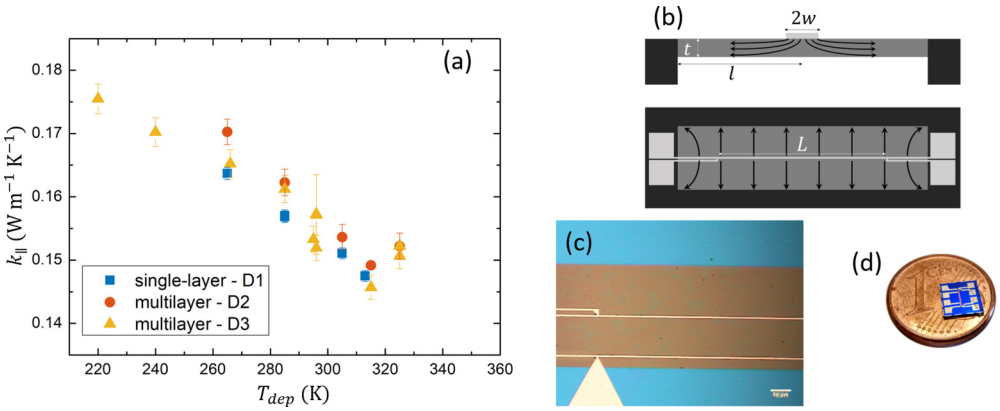

FIG. 2. Heater/sensors for 3ω-Völklein thermal conductivity and measured values for TPD. (a) Thermal conductivity vs deposition temperatures in TPD glasses. Data points correspond to two different measurement procedures as further explained in Methods. Blue-square points were determined from single independent evaporations and cleaning the sensor after each measurement. Triangles and circles correspond to data obtained with a continuous method using two different devices, in which multilayers are deposited sequentially and the differential conductance provides values for each individual layer. (b) Schematic design of the sensor and the direction of the heat flow. (c) Optical images of membrane (brown) and the heater/sensor (central metallic line) and upper view of the chip (d).

which relates the ensemble average of the autocorrelation of the heat current vector $\vec{J}$ to the thermal conductivity. In this equation, T and V are, respectively, the system temperature and volume; k_B is the Boltzmann constant and the index α labels Cartesian components. The heat current is evaluated through its virial expression [6]

$$\vec{J}(t) = \frac{d}{dt}\sum_i \vec{r}_i(t)e_i,$$

where e_i is the per-atom energy (potential and kinetic) of the ith particle and $\vec{r}_i$ is the corresponding position. For the here adopted force fields, the evaluation of $\vec{j}(t)$ requires the calculation of a kinetic energy contribution, a pairwise energy contribution, and a reciprocal-space contribution from long-range Coulomb interactions (as well as similar terms for the bond, angle, dihedral, and improper energy contributions looped over all the atomic pairs, triplets, and quadruplets). Details about the calculation of the above Green-Kubo integral are provided at Ref. [50].

III. RESULTS AND DISCUSSION

A. Dependence of the thermal conductivity on deposition temperature

The in-plane thermal conductivity $k_{\parallel}$ of the vapor-deposited films was evaluated by the modified 3ω-Völklein technique [46–49], while through-plane, $k_{\perp}$, measurements were carried out using the 3ω method developed by Cahill and coworkers [56]. The experimentally measured in-plane thermal conductivity of the TPD layers is presented as a function of the deposition temperature in Fig. 2(a). Similar results obtained with N,N′-bis(1-naphthyl)-N,N′-diphenyl-1,1′-biphenyl-4,4′-diamine (α-NPD) glassy films are shown in Supplemental Material (Fig. S1 in Ref. [50]). Schematics of the 3ω-Völklein and the membrane-based chip used in the measurements are shown in Figs. 2(b)–2(d). All measurements were carried out in high vacuum at a fixed temperature of 296 K. The different symbols of Fig. 2(a) correspond to measurements on various samples following different, but comparable, measurement protocols, as explained in the Methods section. The low values of the in-plane thermal conductivity $\approx$0.16 W m^{-1} K^{-1} are a preliminary indication of the amorphous character of the layers and that heat is mainly carried by atomic vibrations that, in such systems, are mostly localized (i.e., have quite a short mean free path). $k_{\parallel}$ decreases first from 0.175 W m^{-1} K^{-1} ($T_{\rm dep}$ = 220 K, 0.66 $T_{\rm g}$) to 0.147 W m^{-1} K^{-1} ($T_{\rm dep}$ = 315 K, 0.94 $T_{\rm g}$) and then increases to 0.152 W m^{-1} K^{-1} ($T_{\rm dep}$ = 325 K, 0.98 $T_{\rm g}$). We note that we were unable to resolve with enough accuracy the thermal conductivity for samples deposited very close to $T_{\rm g}$ and those points are not shown in Fig. 2. The whole data set is plotted in Fig. S2 of Ref. [50]. The main reason for the lack of reproducibility close to $T_{\rm g}$ may be related to the high surface mobility and the specific geometry of our sensor that consists of a narrow channel (SiN_x membrane) with sharp Si walls at the edges (see schematics of Figs. 2(b) and S4 in Ref. [50]), conditions that favor the dewetting of the layer from the early stages. In this case, the uncertainty in the amount of mass sensed produces low accuracy and reproducibility of the thermal conductivity. At temperatures below 325 K, the measurements at different temperatures were reproducible with an uncertainty of $\pm$0.004 W m^{-1} K^{-1}. The major sources of uncertainty are coming from the determination of the evaporated thickness and the geometrical dimensions of the heater/sensor.

Interestingly enough, the dependence of the in-plane thermal conductivity with the deposition temperature is in line with several previous studies providing evidence that the properties of vapor deposited organic glasses can be tailored by tuning the deposition conditions [13,22,23,57]. In particular, the highest densities and thermal and kinetic stabilities are achieved at deposition temperatures in the vicinity of 0.85 $T_{\rm g}$. TPD has a maximum in stability and density at 285 K (0.85 $T_{\rm g}$), above and below this temperature, both the density and the stability decrease [14]. Typical calorimetric traces for TPD glasses are

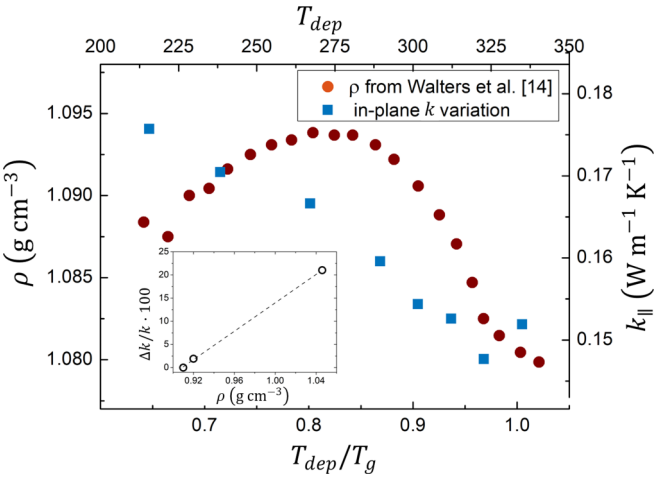

FIG. 3. Thermal conductivity compared to the density of the stable glasses. Thermal conductivity and density variation in TPD as a function of deposition temperature relative to the glass transition temperature. Density data taken from Walters *et al.* [14] assuming a density of 1.08 g/cm^3 for the conventional liquid. (Inset) MD simulations of the role of density in the thermal conductivity of an isotropic glass.

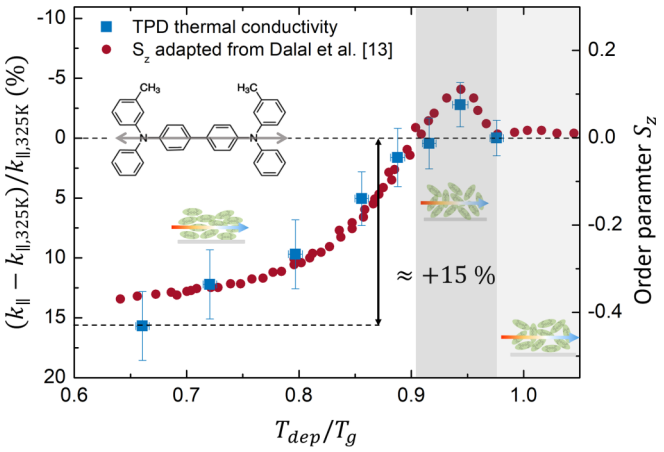

FIG. 4. Correlation between thermal conductivity and molecular orientation. Comparison between the relative variation of the thermal conductivity and the order parameter obtained from Dalal *et al.* [13] plotted against the deposition temperature scaled by T_g.

plotted in Fig. S3 (Ref. [50]) showing the enhanced stability. Films grown at around 0.85 T_g show both an increase of the onset of devitrification, T_{on}, during heating scans and a larger overshoot at T_{on}, clear signatures of their enhanced kinetic and thermodynamic stability.

In order to understand if the observed variation of the in-plane thermal transport correlates to changes in the density of the glassy films, we plot in Fig. 3 this variable obtained from Ref. [14] (red-circles, left axis) together with the in-plane thermal conductivity (blue squares, right axis) versus T_{dep}. It is readily apparent from this figure that density and thermal conductivity do not correlate over the substrate temperatures explored here. While the denser glasses are obtained at $T_{dep} \approx 0.80$–$0.85\,T_g$, the maximum value of thermal conductivity is reached at 0.66 T_g (approximately 220 K). In fact, an increase in density should be followed by an increase in thermal conductivity and not the contrary, as clearly occurs in the region 0.65–0.85 T_g. The inset in Fig. 3 sheds light on this assumption by plotting the relative k, determined from Green Kubo molecular dynamic simulations, versus the density of several isotropic glasses spanning more than 15% in density variation. The formation of these simulated glasses is explained in the Methods, Ref. [50], and shown in Fig. S5, though we remark that the molecular unit is built with the consistent valence force field (CVFF) to take account of intramolecular interactions and by a superposition of a Lennard-Jones potential and a Coulomb term for the nonbonded interactions. From these data, a 1.5% increase in density should produce an increase of the thermal conductivity by around 2.5%. On the contrary, the experimental data show that a glass grown at 220 K with a density lower by 0.4% with respect to a glass grown at 315 K undergoes an increase of the thermal conductivity by 15%. The lack of correlation between thermal conductivity and density indicates that there might be some other factor accounting for the thermal conductivity variation with T_{dep}.

B. Influence of molecular packing

Figure 4 shows the relative variation of $k_\parallel$ (blue squares, left-axis) normalized to the 325 K value, 0.152 ± 0.004 W m^{-1} K^{-1}. In red circles (right axis), the order parameter S_z extracted from Dalal *et al.* [13] is plotted in the same figure with a common x axis. The order parameter S_z is a measure of the average orientation of the molecules. It is defined as $S_z = (3\langle\cos^2\theta_z\rangle - 1)/2$, where θ_z is the angle of the long molecular axis relative to the substrate normal. Its definition is such that the $S_z = -0.5$, 0, or 1.0 value is, respectively, indicating that all the molecules are oriented parallel to the plane of the substrate, a totally random orientation, or a perfect vertical alignment. The correlation between S_z and the thermal conductivity variation is remarkably good as seen from Fig. 4. When the molecules are in preference horizontally oriented ($T_{dep} < 290$ K), the in-plane thermal conductivity is higher. It is worth noticing that even the small peak of S_z at 315 K (0.95 T_g), indicating a small tendency to vertical orientation, is reproduced in the thermal conductivity data. Our results suggest that heat transport in the parallel direction is favored when molecules tend to lie with the long molecular axis (along the N-N axis) parallel to the surface (see sketches in Fig. 4). On the contrary, in-plane thermal transport is sizably reduced when molecules tend to align along the out-of-plane direction. At first glance, this is somewhat surprising given the small size of the molecular unit and the disorder inherent to the glass that should minimize the influence of molecular orientation. To confirm the existence of thermal anisotropy, we carried out through-plane thermal conductivity measurements with the 3ω technique on two TPD samples, one grown at $T_{dep} = 220$ K with the molecules preferentially aligned parallel to the substrate and another at $T_{dep} = 304$ K with isotropic orientation. The results are summarized in Fig. 5. Since we were mostly interested on the relative variation of the thermal conductivity between both samples, we did not carry thickness dependent measurements

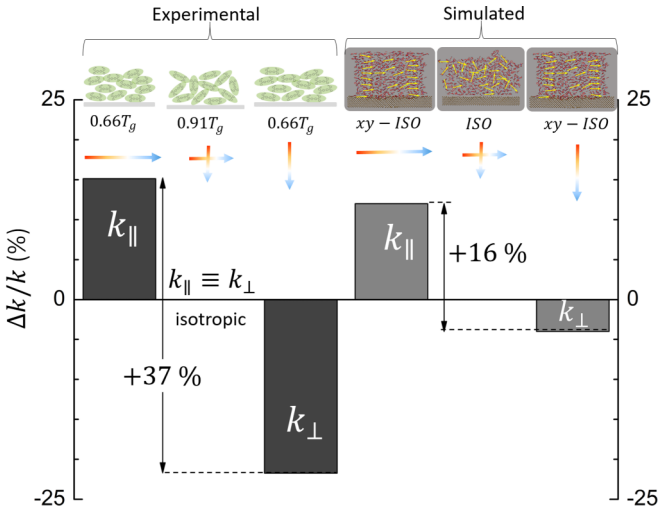

FIG. 5. Thermal anisotropy ratio for experimental and simulated samples. Schematics showing the relative variation of thermal conductivity for the various experimental (left) and simulated (right) samples. Sample grown at 220 K (approximately 0.66 T_g) is roughly equivalent to the simulated *xy-ISO*. The upper panel illustrates the structure of the experimental and simulated samples. The colored arrows indicate the direction of the heat flux. The yellow arrows in the simulated samples indicate the long molecular axis.

to remove the influence of the thermal interface resistance between dissimilar layers. Since both samples have the same thickness and similar thermal interface barriers, the relative difference is accurate enough to provide a suitable description. For the sample grown at 220 K, we got a $k_\perp$ 22% lower than in the isotropic film. This result agrees with the previous in-plane measurements (Fig. 3) and the influence of the molecular packing anisotropy since thermal transport in the perpendicular direction is low when molecules lie roughly parallel to the substrate, i.e., when $k_\parallel$ is maximal. Therefore, considering that the isotropic sample has identical parallel and perpendicular conductivities, we obtain a value of the thermal anisotropy ratio measured at a T = 220 K of $\simeq$37% (Fig. 5).

In order to underpin the effect of the molecular packing anisotropy on thermal transport in organic glasses, we carried out extensive molecular dynamics simulations on a system with tailored orientation of the TPD molecules (see Fig. S5 for more details about the structure). A set of computational samples (Fig. 5 upper panel and Fig. S5) with density values similar to the experimental ones (see Ref. [50] for details) and different packing arrangements was built to mimic the low-temperature vapor deposited ones. Specifically, we generated three unlike samples differing for their main molecular orientation. The *ISO* sample was obtained simply by quenching from the melt and, therefore, it becomes fully isotropic or, equivalently, it does not show any preferential alignment of TPD molecular axes. The remaining two samples, respectively referred to as *xy-ISO* and *ANIS*, were both characterized by a preferential in-plane molecular orientation, where the reference plane is in any case the substrate surface: this feature has been obtained by enforcing the planar alignment of molecular axis during the sample preparation. However, the two systems differ in that the in-plane alignment is totally random in the *xy-ISO* sample or further enforced to align the x direction for the *ANIS* sample, respectively. In short, the sequence *(ISO)-(xy-ISO)-(ANIS)* provides an increasing character of molecular anisotropy. A quantitative analysis of the molecular packing orientation in the simulated samples and the calculated X-ray diffraction pattern is presented in Ref. [50]. The relative difference between the thermal conductivity of the *xy-ISO* sample in the in-plane direction and the corresponding through-plane value is 16%, in qualitative agreement with the experimental data, as shown in Fig. 5. Sample *ANIS* shows an even higher thermal anisotropy ratio between $k_{\parallel,x}$ (in-plane along x) and the through-plane thermal conductivity of 95%.

Our results (both modeling and experimental data) indicate that the variations of thermal conductivity are mainly driven by the molecular packing anisotropy while density plays a minor role. This is in contrast to very recent measurements of electronic transport on vapor-deposited α-NPD films [56], in which increasing film density was more effective to enhance the electrical performance than controlling molecular orientation.

In the organic semiconductor studied here, thermal transport along the N-N backbone of the TPD molecule is preferred with respect to transport along the direction perpendicular to the phenyl rings. We propose that this effect could be interpreted in terms of a different efficiency in transmitting heat carriers, depending on the direction of the heat flow with respect to the molecular orientation. In order to substantiate this conjecture, we simulated two different quasi-1D structures, namely (i) a linear bundle of TPD molecules aligned along the N-N axis and (ii) a line-up of TPD molecules aligned along the direction of π-π bonding. Hereafter, we will refer to such configurations as backbone stacking or π-π stacking, respectively. They are shown in the upper panel of Fig. 6 together with a plot of the thermal conductivity versus length for the linear chains, Fig. 6(a). The overall trend shows a saturation for increasing length and confirms that the direction perpendicular to the backbone is detrimental for heat transport. Present simulations intelligibly reported a 70% higher thermal conductivity for the backbone configuration. In order to explain this result, we have calculated the interaction strength between molecules in both stacking arrangements as function of the inter-molecular spacing. More specifically, the average inter-molecular distance $\langle r_{\text{inter}} \rangle$ was varied in the range 4.75 Å $\leqslant$ $r_{\text{inter}} \leqslant$ 7.5 Å and the corresponding configurational energy has been computed as shown in Fig. 6(b). Such a potential energy nearby the equilibrium distance is basically harmonic, while at smaller/higher distances the onset of anharmonic behavior is observed, as expected. A parabolic fitting near the minimum yields the effective force constants characterizing the intermolecular coupling within a simple spring-and-ball picture. The quadratic fit for both set of data is a function of the form $f(x) = K(x-x_0)^2 + C$, where K is the spring constant and C is the energy minimum located at x_0. The obtained values are $K_{\text{backbone}} = 824.7\,\text{kcal mol}^{-1}\,\text{Å}^{-2}$, $X_{0,\text{backbone}} = 6.39$ Å, and $C_{\text{backbone}} = 5047.2$ kcal/mol, for the backbone configuration and $K_{\text{stacking}} = 312.7\,\text{kcal/mol}^{-1}\,\text{Å}^{-2}$, $X_{0,\text{stacking}} = 5.67$ Å, and $C_{\text{stacking}} = 5202.8$ kcal/mol for the stacking configuration. Consistently with the adopted picture, we argue a stiffer effective spring value translates into a more efficient

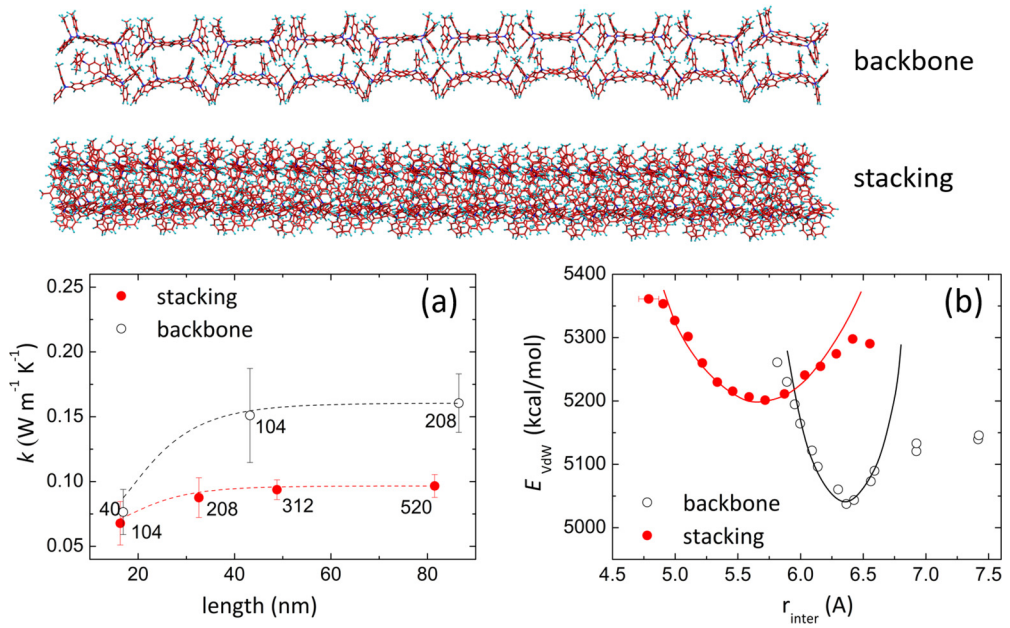

FIG. 6. Thermal conductivity and van der Waals energy of simulated quasi-1D structures. (Top) Backbone and stacking quasi-1D structures. (Bottom) (a) Thermal conductivity vs length for the quasi-1D structures. (b) Configurational energy due to van der Waals interactions vs intermolecular spacing.

thermal conduction, according to the following twofold heuristic argument. In general, thermal conductivity is proportional to the group velocity of heat carriers: since a larger force constant causes a steeper vibrational branch, this reflects into a higher group velocity. On the other hand, we understand that heat current basically represents the energy transferred by a flux of carriers corresponding to atomic vibrations: the higher the force constant, the higher the vibrational and, therefore the energy of such heat carriers. We note that the thermal anisotropy reported here qualitatively agrees with observations in aligned polymers systems where an increase in the strength of intermolecular forces leads to an enhancement of the thermal conductivity [44].

The in-plane and through-plane conductance can be estimated considering that the molecules and vdW interactions form a thermal resistive network, as shown in Fig. 7. We assume that the interfacial thermal resistance (ITR) that corresponds somehow to the coupling between neighboring molecules that are joined through weak van der Waals interactions dominates thermal transport. A stronger molecular interaction is represented by a lower *ITR* (higher thermal interface conductance, TIC) and the intermolecular π-π stacking entails a higher thermal resistance between molecules. According to Fourier's law, the heat flux, Q, is proportional to the temperature difference ΔT, $Q = G^*\Delta T$, where G is the thermal conductance. If the series *ITR* dominate heat transfer, G will be equal to the thermal interface conductance due to vdW interactions and the thermal conductivity may be simply written as $k = L/G_{\mathrm{vdW}}$, where L is the average distance between molecules (see Ref. [50] for details about the calculation). To estimate values of in-plane and through-plane G_{vdW}, we take the average distance between molecules evaluated through the x-ray diffraction patterns of the simulated samples (see Ref. [50] for more details about the x-ray profiles). The obtained values $L_{\parallel} = 6.0 \pm 0.2$ Å and $L_{\perp} = 4.58 \pm 0.2$ Å are in excellent agreement with experimental data measured by Gujral *et al.* [58]. Using the experimental values of the thermal conductivities, $k_{\parallel} = 0.175$ W m^{-1}K^{-1} and $k_{\perp} = 0.110$ W m^{-1}K^{-1}, gives $G_{\mathrm{vdW},\parallel} \approx 300$ MW m^{-2}K^{-1} and $G_{\mathrm{vdW},\perp} \approx 230$ MW m^{-2}K^{-1}. We note that given the inherent disorder of the samples the evaluated conductance should be considered as an average contribution to the thermal boundary conductance of the various vdW interactions between different entities of nearest-neighbor molecules and therefore cannot be directly compared to the directional force constants evaluated previously. Although a direct comparison to previous TIC values on other systems is problematic due to the impact of disorder on our data, we provide a comparison to previous works. Our values are significantly lower than those reported for metal/dielectric interfaces, approximately 1 GW m^{-2}K^{-1} and comparable to the calculated TIC between different

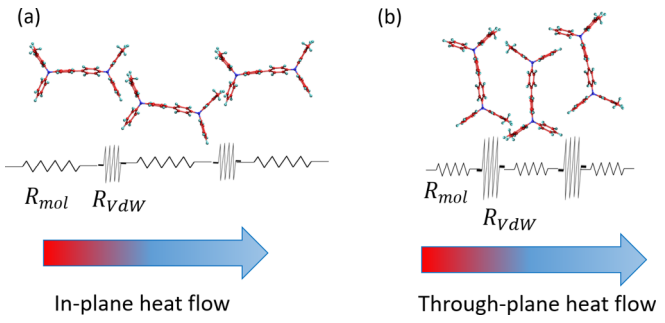

FIG. 7. Thermal resistive network. Schematics of thermal resistance network in the in-plane direction (a) and the through-plane direction (b). R_{vdW} accounts for the strength of the intermolecular interactions and R_{mol} represents the intramolecular thermal resistance.

crystallographic orientations in crystalline dinaphtho[2,3-b:2′,3′-f]thieno[3,2-b]thiophene (DNTT) that ranges from 150–300 MW m^{-2} K^{-1} [59] or to the interface between myoglobin proteins that amounts to 301 MW m^{-2} K^{-1} at 320 K [60]. The data for TPD lie between those of organic-organic interfaces such as copper phthalocyanine (CuPc)–fullerene (C60) interfaces, (TIC ≈ 400 MW m^{-2} K^{-1}) and organic/inorganic interfaces such as pentacene/metal (TIC ≈ 10 MW $m^{-2}K^{-1}$) [61] or CuPc-Au (TIC ≈ 20 MW m^{-2} K^{-1}), that is purely a vdW-like interaction [62].

IV. CONCLUSION

In summary, we have demonstrated that heat transport in vapor deposited glassy films of TPD is ruled by the molecular orientation while density plays a minor role. Our results show that the in-plane thermal conductivity of vapor deposited thin film stable glasses of TPD strongly depends on the deposition temperature and a thermal anisotropy ratio of ≈40% is achieved at a T_{dep} of 220 K (0.66 T_g). At this temperature, molecules are on average located with the phenyl rings perpendicular to the growth direction and there is a strong anisotropy between the in-plane and through-plane directions. This packing anisotropy has a strong effect in heat propagation. The microscopic details of heat transport are revealed by molecular dynamics simulations that show the different strengths of the molecular interaction in the direction along the backbone of the molecules compared to the direction of the π-π stacking. The stronger molecular interaction along the backbone favors the propagation of microscopic heat carriers along this direction. This is at odds with electronic transport that favors propagation along the perpendicular direction to the long axis of the molecule provided there is sufficient π-π interaction. This strategy could be employed in future developments of OLED devices to minimize formation of hot spots or to implement small molecule thin films for its use in thermoelectric-based applications.

ACKNOWLEDGMENTS

This work was financially supported by the Spanish Ministry of Economy and Competitiveness (MINECO) under contract Projects MAT2013-40896-P and MAT2016-79579-R together with the European Regional Development Funds (ERDF). P. Ferrando-Villalba and J. Ràfols-Ribé were also in receipt of a FPU grant from the Spanish Ministry of Education, Culture and Sport at the time of the study. Ll. Abad thanks the MINECO for a Ramón y Cajal Contract (RYC-2013-12640) and CSIC for JAE-INTR_14_00479.

[1] C. A. Angell, Science **267**, 1924 (1995).
[2] B. Geffroy, P. le Roy, and C. Prat, Polym. Int. **55**, 572 (2006).
[3] S. Reineke, M. Thomschke, B. Lüssem, and K. Leo, Rev. Mod. Phys. **85**, 1245 (2013).
[4] J. R. Sheats, H. Antoniadis, M. Hueschen, W. Leonard, J. Miller, R. Moon, D. Roitman, and A. Stocking, Science **273**, 884 (1996).
[5] X. Zhou, J. He, L. S. Liao, M. Lu, X. M. Ding, X. Y. Hou, X. M. Zhang, X. Q. He, and S. T. Lee, Adv. Mater. **12**, 265 (2000).
[6] S. Chung, J.-H. Lee, J. Jeong, J.-J. Kim, and Y. Hong, Appl. Phys. Lett. **94**, 253302 (2009).
[7] X. Wang, K. D. Parrish, J. A. Malen, and P. K. L. Chan, Sci. Rep. **5**, 16095 (2015).
[8] O. Bubnova, Z. U. Khan, A. Malti, S. Braun, M. Fahlman, M. Berggren, and X. Crispin, Nat. Mater. **10**, 429 (2011).
[9] Q. Zhang, Y. Sun, W. Xu, and D. Zhu, Adv. Mater. **26**, 6829 (2014).
[10] T.-A. Lin, T. Chatterjee, W.-L. Tsai, W.-K. Lee, M.-J. Wu, M. Jiao, K.-C. Pan, C.-L. Yi, C.-L. Chung, K.-T. Wong, and C.-C. Wu, Adv. Mater. **28**, 6976 (2016).
[11] D. Mendels and N. Tessler, J. Phys. Chem. Lett. **5**, 3247 (2014).
[12] K. P. Pernstich, B. Rössner, and B. Batlogg, Nat. Mater. **7**, 321 (2008).
[13] S. S. Dalal, D. M. Walters, I. Lyubimov, J. J. de Pablo, and M. D. Ediger, Proc. Natl. Acad. Sci. USA **112**, 4227 (2015).
[14] D. M. Walters, R. Richert, and M. D. Ediger, J. Chem. Phys. **142**, 134504 (2015).
[15] K. L. Kearns, S. F. Swallen, M. D. Ediger, T. Wu, and L. Yu, J. Chem. Phys. **127**, 154702 (2007).
[16] E. Leon-Gutierrez, A. Sepúlveda, G. Garcia, M. T. Clavaguera-Mora, and J. Rodríguez-Viejo, Phys. Chem. Chem. Phys. **18**, 8244 (2016).
[17] M. Ahrenberg, Y. Z. Chua, K. R. Whitaker, H. Huth, M. D. Ediger, and C. Schick, J. Chem. Phys. **138**, 024501 (2013).
[18] S. L. L. M. Ramos, M. Oguni, K. Ishii, and H. Nakayama, J. Phys. Chem. B **115**, 14327 (2011).
[19] C. Rodríguez-Tinoco, M. Gonzalez-Silveira, J. Ràfols-Ribé, G. Garcia, and J. Rodríguez-Viejo, J. Non. Cryst. Solids **407**, 256 (2015).
[20] K. R. Whitaker, M. Ahrenberg, C. Schick, and M. D. Ediger, J. Chem. Phys. **137**, 154502 (2012).
[21] K. L. Kearns and S. F. Swallen, J. Phys. Chem. B **113**, 1579 (2009).
[22] E. Leon-Gutierrez, A. Sepúlveda, G. Garcia, M. T. Clavaguera-Mora, and J. Rodríguez-Viejo, Phys. Chem. Chem. Phys. **12**, 14693 (2010).
[23] S. S. Dalal, Z. Fakhraai, and M. D. Ediger, J. Phys. Chem. B **117**, 15415 (2013).
[24] K. Ishii, H. Nakayama, S. Hirabayashi, and R. Moriyama, Chem. Phys. Lett. **459**, 109 (2008).
[25] S. S. Dalal, A. Sepúlveda, G. K. Pribil, Z. Fakhraai, and M. D. Ediger, J. Chem. Phys. **136**, 204501 (2012).
[26] Y. Z. Chua, M. Ahrenberg, M. Tylinski, M. D. Ediger, and C. Schick, J. Chem. Phys. **142**, 054506 (2015).
[27] K. J. Dawson, K. L. Kearns, M. D. Ediger, M. J. Sacchetti, and G. D. Zografi, J. Phys. Chem. B **113**, 2422 (2009).
[28] K. L. Kearns, T. Still, G. Fytas, and M. D. Ediger, Adv. Mater. **22**, 39 (2010).
[29] J. Ràfols Ribé, *Organic Vapour -Deposited Stable Glasses: From Fundamental Thermal Properties to High-Performance Organic Light-Emitting Diodes*, Universitat Autònoma de Barcelona, 2017, http://www.tesisenred.net/handle/10803/457956.
[30] T. D. Schmidt, T. Lampe, D. Sylvinson M. R., P. I. Djurovich, M. E. Thompson, and W. Brütting, Phys. Rev. Appl. **8**, 037001 (2017).

[31] H.-W. Lin, C.-L. Lin, H.-H. Chang, Y.-T. Lin, C.-C. Wu, Y.-M. Chen, R.-T. Chen, Y.-Y. Chien, and K.-T. Wong, J. Appl. Phys. **95**, 881 (2004).

[32] D. Yokoyama, A. Sakaguchi, M. Suzuki, and C. Adachi, Appl. Phys. Lett. **93**, 173302 (2008).

[33] D. Yokoyama, J. Mater. Chem. **21**, 19187 (2011).

[34] M. D. Ediger, J. Chem. Phys. **147**, 210901 (2017).

[35] S. Fratini, S. Ciuchi, D. Mayou, G. T. de Laissardière, and A. Troisi, Nat. Mater. **16**, 998 (2017).

[36] N. Kim, B. Domercq, S. Yoo, A. Christensen, B. Kippelen, and S. Graham, Appl. Phys. Lett. **87**, 241908 (2005).

[37] N. Lu, L. Li, N. Gao, and M. Liu, Org. Electron. **41**, 294 (2017).

[38] C. J. Glassbrenner and G. A. Slack, Phys. Rev. **134**, A1058 (1964).

[39] D. G. Cahill, M. Katiyar, and J. R. Abelson, Phys. Rev. B **50**, 6077 (1994).

[40] D. G. Cahill and R. O. Pohl, Solid State Commun. **70**, 927 (1989).

[41] H. Zhang and J. W. Brill, J. Appl. Phys. **114**, 043508 (2013).

[42] H. Zhang, Y. Yao, M. M. Payne, J. E. Anthony, and J. W. Brill, Appl. Phys. Lett. **105**, 073302 (2014).

[43] K. Kurabayashi, M. Asheghi, M. Touzelbaev, and K. E. Goodson, J. Microelectromechanical Syst. **8**, 180 (1999).

[44] V. Singh, T. L. Bougher, A. Weathers, Y. Cai, K. Bi, M. T. Pettes, S. A. McMenamin, W. Lv, D. P. Resler, T. R. Gattuso, D. H. Altman, K. H. Sandhage, L. Shi, A. Henry, and B. A. Cola, Nat. Nanotechnol. **9**, 384 (2014).

[45] A. Weathers, Z. U. Khan, R. Brooke, D. Evans, M. T. Pettes, J. W. Andreasen, X. Crispin, and L. Shi, Adv. Mater. **27**, 2101 (2015).

[46] A. Sikora, H. Ftouni, J. Richard, C. Hébert, D. Eon, F. Omnès, and O. Bourgeois, Rev. Sci. Instrum. **83**, 054902 (2012).

[47] A. Sikora, H. Ftouni, J. Richard, C. Hébert, D. Eon, F. Omnès, and O. Bourgeois, Rev. Sci. Instrum. **84**, 029901 (2013).

[48] P. Ferrando-Villalba, D. Takegami, L. Abad, J. Ràfols-Ribé, A. Lopeandía, G. Garcia, and J. Rodriguez-Viejo, arXiv:1803.06275.

[49] F. Völklein and T. Starz, *Proceedings of the 16th International Conference on Thermoelectrics, Dresden, Germany* (IEEE, Piscataway, NJ, 1997), p. 711.

[50] See Supplemental Material at http://link.aps.org/supplemental/10.1103/PhysRevMaterials.2.035603 for details of the experimental evaluation of the thermal conductivity, the generation of the simulated samples (density and structure), and the calculation of the thermal conductivity.

[51] P. DauberOsguthorpe, V. A. Roberts, D. J. Osguthorpe, J. Wolff, M. Genest, and A. T. Hagler, Proteins Struct. Funct. Bioinforma. **4**, 31 (1988).

[52] C. I. Bayly, P. Cieplak, W. Cornell, and P. A. Kollman, J. Phys. Chem. **97**, 10269 (1993).

[53] W. D. Cornell, P. Cieplak, C. I. Bayly, and P. A. Kollman, J. Am. Chem. Soc. **115**, 9620 (1993).

[54] J. Tersoff, Phys. Rev. B **39**, 5566 (1989).

[55] S. Plimpton, J. Comput. Phys. **117**, 1 (1995).

[56] D. G. Cahill, Rev. Sci. Instrum. **61**, 802 (1990).

[57] S. F. Swallen, K. L. Kearns, M. K. Mapes, Y. S. Kim, R. J. McMahon, M. D. Ediger, T. Wu, L. Yu, and S. Satija, Science **315**, 353 (2007).

[58] A. Gujral, K. A. O'Hara, M. F. Toney, M. L. Chabinyc, and M. D. Ediger, Chem. Mater. **27**, 3341 (2015).

[59] X. Wang, J. Zhang, Y. Chen, and P. K. L. Chan, Nanoscale **9**, 2262 (2017).

[60] D. M. Leitner, J. Phys. Chem. B **117**, 12820 (2013).

[61] J. Epstein, W.-L. Ong, C. J. Bettinger, and J. A. Malen, ACS Appl. Mater. Interfaces **8**, 19168 (2016).

[62] Y. Jin, C. Shao, J. Kieffer, K. P. Pipe, and M. Shtein, J. Appl. Phys. **112**, 093503 (2012).